Perturbation theory for asymmetric deformed microdisk cavities

Julius Kullig and Jan Wiersig
Institut für Theoretische Physik, Otto-von-Guericke-Universität Magdeburg, Postfach 4120, 39016 Magdeburg, Germany
(Received 5 September 2016; published 26 October 2016)

In an article by Dubertrand *et al.* [Phys. Rev. A **77**, 013804 (2008)] the perturbation theory for slightly deformed optical microcavities with a mirror-reflection symmetry was developed. However, in real experiments such a mirror-reflection symmetry is often not present either intended or unintended via production tolerances. In this paper we therefore extended the perturbation theory to asymmetric boundary deformations. Consequently, we are able to describe interesting non-Hermitian phenomena like copropagation of optical modes in the (counter-) clockwise direction inside the cavity. The derived analytic formulas are demonstrated at two generic boundary shapes, the spiral and the double-notched circle where a good agreement to the numerical boundary element method is observed.

DOI: 10.1103/PhysRevA.94.043850

I. INTRODUCTION

Optical microcavities can store light into very small volumes for large times. Therefore, they have been considered and realized for a wide range of applications, e.g., as unidirectional light emitters [1–3], nanoparticle sensors [4–6], optical gyroscopes [7,8], and coupled-resonator optical waveguides [9–12]. An often investigated class of microcavities are quasi-two-dimensional optical microdisks with homogeneous refractive index n. Here, the boundary shape in the x-y plane determines the properties of the optical modes. Analytical solutions can only be obtained for very simple geometries with rotational symmetry. The frequently considered deformed cavities, see Figs. 1(a)–1(d) for some common examples, require an elaborate numerical treatment, e.g., with the boundary element method (BEM) [13]. However, these deformed cavities are of large interest to study wave chaos and non-Hermitian physics of weakly open systems both theoretically and experimentally [14–18].

Therefore, methods to obtain approximate solutions for optical modes have been developed which are based, e.g., on nondegenerate perturbation theory [19–22], semiclassical calculations [23–25], or dynamical tunneling in phase space [26,27]. However, all of these methods are only able to handle cavities with a mirror-reflection symmetry [as shown in Figs. 1(a) and 1(b)] where the modes fall into two orthogonal classes with even and odd parity with respect to the symmetry line. Asymmetric deformations as in Figs. 1(c) and 1(d) are not yet covered by these approximation methods. Note that in an experiment, asymmetric deformations can also develop unintendedly during the production process; see, e.g., Refs. [28,29].

The purpose of this paper is to extend the nondegenerate perturbation theory for slightly deformed optical cavities by Dubertrand *et al.* [19] to a degenerate perturbation theory for asymmetric boundary deformations which violate mirror-reflection symmetry. The derived formulas are analytical and therefore allow for an easy evaluation. The results include interesting non-Hermitian effects of these cavities: optical modes come in nearly degenerate pairs where both modes are not standing waves but aligned traveling waves in either the clockwise (CW) or counterclockwise (CCW) direction [30]. This causes a strong nonorthogonality of the mode pair. At so-called exceptional points (EPs) [31–35] in parameter space the mode pair coalesces, i.e., the modes become collinear with the same complex wave number. This has been considered to enhance the sensitivity of sensors [36] and construct orbital angular momentum microlasers [37,38].

An additional possible application of the derived perturbation theory for asymmetric deformations is the inverse problem for microcavities introduced in Ref. [39]. Here, the task is to optimize the boundary shape of the cavity to get a desired far-field emission pattern. Including the perturbation theory for asymmetric deformations in the inverse problem will allow for an optimization to the more general and asymmetric far-field pattern. This will be part of future investigations.

In this paper we demonstrate the usefulness of the derived formulas at two generic boundary deformations which have previously attracted attention: the spiral [3,30,40–42] [Fig. 1(c)] and a double-notched circle [21,43,44] [Fig. 1(d)]. In both cases we observe a very good agreement with the numerically exact BEM.

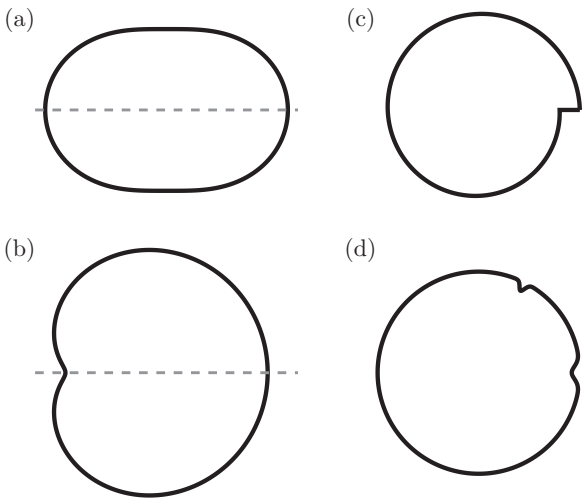

FIG. 1. The boundary of (a),(b) symmetric and (c),(d) asymmetry deformed microcavities is shown as a solid curve. A dashed line illustrates the mirror-reflection symmetry. The cavities are (a) the quadrupole, (b) the Limaçon, (c) the spiral, and (d) the asymmetric double-notched circular cavity.

The paper is organized as follows. An introduction to the mode equation for microdisk cavities is presented in Sec. II. In Sec. III we give a short review on the circular microdisk and its mirror-reflection symmetry preserving deformations. In Sec. IV we present the perturbation theory for slightly but asymmetric deformed microcavities. The application to the spiral and the notched circle is demonstrated in Sec. V. A conclusion and outlook is given in Sec. VI. In the Appendix we present an improvement of the derived formulas using a rescaled cavity size.

II. THE MODE EQUATION

For many investigations of microcavities the detailed knowledge of the stationary electric and magnetic field pattern, the optical modes, is essential. In the case of quasi-two-dimensional optical microdisks, Maxwell's equations reduce to a scalar Schrödinger-type mode equation

$$[\Delta + k^2 n^2(\mathbf{r})]\Psi(\mathbf{r}) = 0 \tag{1}$$

for Ψ representing either the z direction of the magnetic field (transverse electric [TE] polarization) or the electric field (transverse magnetic [TM] polarization). Along the cavities's interface in the x-y plane the boundary conditions

$$\Psi_{\text{in}} = \Psi_{\text{out}} \tag{2}$$

and

$$\partial_\nu \Psi_{\text{in}} = \partial_\nu \Psi_{\text{out}} \quad \text{for TM polarization,} \tag{3a}$$

$$\frac{1}{n_{\text{in}}^2}\partial_\nu \Psi_{\text{in}} = \frac{1}{n_{\text{out}}^2}\partial_\nu \Psi_{\text{out}} \quad \text{for TE polarization} \tag{3b}$$

need to be fulfilled for the normal vector ν. In the following $n = n_{\text{in}}$ is the effective refractive index inside the cavity; outside it is assumed to be $n_{\text{out}} = 1$. In this paper we restrict ourselves to the case of TM polarization.

In combination with the outgoing wave condition

$$\Psi_{\text{out}} \propto h(k,\phi)\frac{\exp(ikr)}{\sqrt{r}} \tag{4}$$

for large r the mode equation (1) is solvable only for discrete values of the complex (dimensionless) wave number $x = kR$ whose real part represents the vacuum wave length $\lambda = 2\pi/(\text{Re}\, k)$ and the imaginary part determines the decay rate of the optical mode inside the cavity with time. Therefore, the quality factor $Q = -\text{Re}\, x/(2\text{Im}\, x)$ characterizes the lifetime of an optical mode.

III. THE CIRCULAR MICROCAVITY AND ITS SYMMETRIC DEFORMATIONS

In the case of the circular optical cavity defined in polar coordinates by

$$r(\phi) = R, \tag{5}$$

Eq. (1) is solved with the ansatz

$$\Psi_{\text{in}}(r,\phi) = \frac{J_m(nkr)}{J_m(nx)}e^{im\phi}, \tag{6a}$$

$$\Psi_{\text{out}}(r,\phi) = \frac{H_m(kr)}{H_m(nx)}e^{im\phi} \tag{6b}$$

for the wave function inside and outside the cavity. Here, J_m and H_m are m-th order Bessel and Hankel functions, both of the first kind. The integer mode number m is associated with the angular momentum of a traveling wave in the CCW direction. Negative m correspond to CW propagation of the mode. Since the boundary conditions (2) and (3a) [(3b) for TE polarization] and the outgoing wave condition (4) need to be fulfilled, the possible values of $x = kR$ are determined as the roots of

$$S_m(x) = n\frac{J_m'}{J_m}(nx) - \frac{H_m'}{H_m}(x), \tag{7}$$

For fixed m, multiple roots $x_{m,l}$ of Eq. (7) exist which are labeled with an integer $l > 0$. This mode number l represents the number of nodes of the wave function in the radial direction.

Modes with $(\pm m,l)$ (except for $m = 0$) are degenerate in their x. Therefore, a transformation from the traveling wave basis (6a) and (6b) with $\pm m$ into a standing wave basis are again solutions of Eq. (1). This standing wave basis represents modes with even and odd parity with respect to the mirror-reflection symmetry line $y = 0$. In the standing wave basis the mode number m is related to the number of nodes of the wave function in the azimuthal direction.

For slight deformations of the circular boundary it is convenient to expand the modes of the deformed cavity in modes of the circular cavity as

$$\Psi_{\text{in}}(r,\phi) = \sum_{p=-\infty}^{\infty} \alpha_p \frac{J_p(nkr)}{J_p(nx)}e^{ip\phi}, \tag{8a}$$

$$\Psi_{\text{out}}(r,\phi) = \sum_{p=-\infty}^{\infty} \beta_p \frac{H_p(kr)}{H_p(nx)}e^{ip\phi}. \tag{8b}$$

If the sums contain a dominant contribution for $\alpha_{|p|}$ and $\beta_{|p|}$ with $p = m$, then m is still a good mode number to characterize the mode in the deformed cavity.

If the deformation is symmetric as in Ref. [19] such that a mirror-reflection symmetry (at $y = 0$) exists also the mode needs to be symmetric, i.e., $|\alpha_{-p}| = |\alpha_p|$. Therefore, modes are separated into two orthogonal classes with even and odd parity. For fixed mode numbers (m,l) the modes with even and odd parity show a small splitting in x due to a coupling between CW and CCW wave propagation.

The perturbation theory for slightly deformed microcavities with a symmetric boundary [19] uses the standing wave basis for unperturbed eigenstates of the circular cavity.

IV. PERTURBATION THEORY FOR ASYMMETRIC DEFORMED MICROCAVITIES

In this section we derive the perturbative approach to asymmetric deformed cavities and present our central formulas. In Sec. IV A we setup our general framework for treating asymmetric boundary deformation in a perturbative way for TM polarized modes. Next, we derive the formulas for first- and second-order perturbation theory in Secs. IV B and IV C, respectively.

A. General setup for the perturbation theory

The perturbation theory assumes that the boundary of the deformed cavity can be written in polar coordinates as

$$r(\phi) = R + \lambda f(\phi), \tag{9}$$

where $|\lambda f(\phi)| \ll R$ represents a small perturbation to the circular cavity, Eq. (5). The area δa where the refractive index is changed by $\lambda f(\phi)$ deals as a measure for the strength of the perturbation. Therefore, one expects reasonable results if the formal criteria

$$s_n \frac{\delta a}{8\pi} (n \mathrm{Re}\, k)^2 \ll 1, \tag{10}$$

with

$$s_n = 1 - \frac{\pi}{2}\left(\arcsin\frac{1}{n} + \frac{1}{n}\sqrt{1-\frac{1}{n^2}}\right) \tag{11}$$

is fulfilled [19]. This criteria is not too strict and reliable results can also be achieved for larger perturbations [20].

Note that we demand the deformation function $f(\phi)$ to be single-valued almost everywhere, but in contrast to Ref. [19] we will employ no symmetry for $f(\phi)$, i.e., $f(\phi) \neq f(-\phi)$. The perturbation parameter λ is assumed to be formally small so that it is valid to solve the mode equation (1) with the boundary conditions (2) and (3a) in powers of λ. For this purpose we write the mode of the deformed cavity which is characterized by the mode numbers (m,l) as

$$\begin{aligned}\Psi_{\mathrm{in}}(r,\phi) &= e^{iz}\frac{J_m(nkr)}{J_m(nx)}e^{im\phi} + e^{-iz}\frac{J_m(nkr)}{J_m(nx)}e^{-im\phi} \\ &\quad + \sum_{p\neq\pm m} a_p \frac{J_p(nkr)}{J_p(nx)} e^{ip\phi}, \end{aligned} \tag{12a}$$

$$\begin{aligned}\Psi_{\mathrm{out}}(r,\phi) &= e^{iz}(1+b_m)\frac{H_m(kr)}{H_m(x)}e^{im\phi} \\ &\quad + e^{-iz}(1+b_{-m})\frac{H_m(kr)}{H_m(x)}e^{-im\phi} \\ &\quad + \sum_{p\neq\pm m}(a_p+b_p)\frac{H_p(kr)}{H_p(x)}e^{ip\phi}. \end{aligned} \tag{12b}$$

In this ansatz the unknown quantities are $x = kR$, z, a_p, and b_p with $p \in \mathbb{Z}$. Especially, the parameter $z \in \mathbb{C}$ fixes the contributions of unperturbed modes with $\pm m$ which are degenerate in the circular cavity. We therefore use the terms $e^{\pm iz}$ for symmetrizing the ansatz so that replacing m with $-m$ enforce replacing z with $-z$ to get the same mode. Note that the wave function as written above is not normalized.

The mode equation (1) and the outgoing wave condition (4) are formally solved with the ansatz (12a) and (12b) but fulfilling the boundary conditions (2) and (3a) requires further investigation. Therefore, we expand them in a power series in λ which gives

$$\begin{aligned}[\Psi_{\mathrm{in}} - \Psi_{\mathrm{out}}](R,\phi) &= -\lambda f(\phi)\partial_r[\Psi_{\mathrm{in}} - \Psi_{\mathrm{out}}](R,\phi) \\ &\quad - \frac{1}{2}\lambda^2 f^2(\phi)\partial_r^2[\Psi_{\mathrm{in}} - \Psi_{\mathrm{out}}](R,\phi) \\ &\quad + O(\lambda^3), \end{aligned} \tag{13a}$$

$$\begin{aligned}\partial_r[\Psi_{\mathrm{in}} - \Psi_{\mathrm{out}}](R,\phi) &= -\lambda f(\phi)\partial_r^2[\Psi_{\mathrm{in}} - \Psi_{\mathrm{out}}](R,\phi) \\ &\quad - \frac{1}{2}\lambda^2 f^2(\phi)\partial_r^3[\Psi_{\mathrm{in}} - \Psi_{\mathrm{out}}](R,\phi) \\ &\quad + O(\lambda^3). \end{aligned} \tag{13b}$$

Equating the coefficients of these equations in order λ^1 and λ^2 allows us to compute the unknown quantities in Eqs. (12a) and (12b). More precisely we need to expand the unknown quantities in powers of the perturbation parameter λ according to the following scheme:

$$\begin{aligned} x &= x_0 + \lambda x_1 &&+ \lambda^2 x_2 &&+ O(\lambda^3), \\ z &= z_0 + \lambda z_1 &&+ O(\lambda^2), \\ a_p &= &&\lambda a_p^{(1)} + \lambda^2 a_p^{(2)} &&+ O(\lambda^3), \\ b_p &= &&\lambda^2 b_p^{(2)} &&+ O(\lambda^3). \end{aligned} \tag{14}$$

Calculating the coefficients in the scheme allows us to determine the wave functions in- and outside the cavity [(12a), (12b)]. This is done in Secs. IV B and IV C.

Note that the term $b_p^{(1)}$ is absent in the scheme (14) which follows from inserting Eq. (13b) into Eq. (13a). Also, the parameter z is just fixed up to $z \sim \lambda^1$ within second-order perturbation theory. Computing the order $z \sim \lambda^2$ would require us to expand x up to third order which may be part of future investigations. But in this paper we will show that the scheme (14) is sufficient to give reasonable results for slightly deformed asymmetric cavities.

Once the parameter in the scheme (14) and therefore the wave functions in- and outside the cavity [Eqs. (12a) and (12b)] have been calculated we can investigate further properties of the optical modes: (i) The chirality α_{ch} [42,43,45] which is here defined as

$$\alpha_{\mathrm{ch}} = \frac{\sum_{p>0}|a_p|^2 - \sum_{p<0}|a_p|^2}{\sum_{p>0}|a_p|^2 + \sum_{p<0}|a_p|^2}, \tag{15}$$

with the convention $a_m = e^{iz}$ and $a_{-m} = e^{-iz}$. It describes the propagation of a mode inside the cavity and ranges from $\alpha_{\mathrm{ch}} = -1$ for a pure clockwise propagating mode to $\alpha_{\mathrm{ch}} = 1$ for a pure counterclockwise propagation. For $\alpha_{\mathrm{ch}} = 0$ the mode is a standing wave. And (ii) the far-field $F(\phi)$ or its intensity pattern $|F(\phi)|^2$ can be calculated within perturbation theory from the asymptotic expansion of the Hankel functions as

$$\begin{aligned} F(\phi) &= (1+b_m)e^{iz}\frac{e^{-i\pi m/2}}{H_m(x)}e^{im\phi} \\ &\quad + (1+b_{-m})e^{-iz}\frac{e^{-i\pi m/2}}{H_m(x)}e^{-im\phi} \\ &\quad + \sum_{p\neq\pm m}(a_p+b_p)\frac{e^{-i\pi p/2}}{H_p(x)}e^{ip\phi}. \end{aligned} \tag{16}$$

B. First-order perturbation theory

In this section we derive formulas for the first-order perturbation theory. For this purpose we compare the coefficients in Eq. (13b) which are proportional to λ^1. Note that we therefore need to evaluate

$$g(x) = g(x_0) + \lambda \left.\frac{\partial g}{\partial x}\right|_{x=x_0} + \frac{\lambda^2}{2}\left.\frac{\partial^2 g}{\partial x^2}\right|_{x=x_0} + O(\lambda^3) \tag{17}$$

for $g \in \{J'/J, H'/H\}$ up to first order in λ and

$$e^{\pm iz} = e^{\pm iz_0} \pm \lambda i z_1 e^{\pm iz_0} + O(\lambda^2). \tag{18}$$

After simplification using Eq. (7) we get

$$-(n^2-1)x_1[e^{iz_0}e^{im\phi} + e^{-iz_0}e^{-im\phi}] + \sum_{p\neq\pm m} a_p^{(1)} S_p e^{ip\phi}$$

$$= \frac{f(\phi)}{R} x_0 (n^2-1)[e^{iz_0}e^{im\phi} + e^{-iz_0}e^{-im\phi}]. \tag{19}$$

Here and in the following, $S_p = S_p(x_0)$ is shortened. Using the orthogonality of $e^{\pm im\phi}$ in Eq. (19) and introducing the Fourier harmonics

$$A_q = \frac{1}{2\pi R}\int_0^{2\pi} f(\phi) e^{iq\phi}\,\mathrm{d}\phi \tag{20}$$

of the boundary deformation, see Eq. (9), the system of equations

$$-x_1 e^{iz_0} = x_0[e^{iz_0}A_0 + e^{-iz_0}A_{-2m}], \tag{21a}$$

$$-x_1 e^{-iz_0} = x_0[e^{iz_0}A_{2m} + e^{-iz_0}A_0] \tag{21b}$$

is extracted. The solutions of this system are the first-order results

$$z_0 = -\frac{1}{4}\arg\left(\frac{A_{2m}}{A_{-2m}}\right) + \mu\frac{\pi}{2}, \qquad \mu \in \mathbb{Z} \tag{22}$$

$$x_1 = -x_0[A_0 + e^{-2iz_0}A_{-2m}], \tag{23}$$

where $A_{-2m} = A_{2m}^\star$. Furthermore, using the orthogonality of $e^{ip\phi}$ with $p \neq \pm m$ in Eq. (19), one gets

$$a_p^{(1)} = \frac{(n^2-1)x_0}{S_p}[e^{iz_0}A_{m-p} + e^{-iz_0}A_{-m-p}]. \tag{24}$$

In the following we make some remarks about the first-order results: (i) In Eq. (22) it is sufficient to restrict $\mu \in \{0,1\}$ to describe a mode pair. Other values of μ will predict the same two modes. (ii) z_0 is real and fixes the phase of the involved unperturbed modes with $\pm m$. It does not contribute to a finite chirality; see Eq. (15). (iii) Equation (23) can be rewritten as

$$x_1 = -x_0(A_0 \pm |A_{2m}|). \tag{25}$$

Hence, the first-order results in general lift the degeneracy in x_0 of the mode pair in the unperturbed cavity. But both modes still have the same Q factor since $Q = -\mathrm{Re}\,x/(2\mathrm{Im}\,x)$ and $A_0 \in \mathbb{R}$. (iv) Equation (22) assumes $A_{-2m} = A_{2m}^\star \neq 0$. For nongeneric boundary shapes with vanishing Fourier harmonic A_{-2m}, one cannot fix z_0 in first-order perturbation theory and only one value $x_1 = -x_0 A_0$ is predicted.

C. Second-order perturbation theory

In this section we compare the coefficients proportional to λ^2 in Eqs. (13a) and (13b). This fixes the remaining unknown quantities in the scheme (14).

After employing Eq. (17) for $g \in \{J'/J, H'/H, S_p\}$ and using Eq. (18) we extract

$$\left[-x_2 + \frac{x_1^2}{2x_0}\left(1 + 2x_0\frac{H_m'}{H_m}\right)\right][e^{iz_0}e^{im\phi} + e^{-iz_0}e^{-im\phi}] - \frac{b_m^2}{n^2-1}\frac{H_m'}{H_m}e^{iz_0}e^{im\phi} - \frac{b_{-m}^2}{n^2-1}\frac{H_m'}{H_m}e^{-iz_0}e^{-im\phi}$$

$$-x_1 i z_1[e^{iz_0}e^{im\phi} - e^{-iz_0}e^{-im\phi}] + \frac{1}{n^2-1}\sum_{p\neq\pm m}\left[a_p^{(1)}x_1\frac{\partial S_p}{\partial x} + a_p^{(2)}S_p - b_p^{(2)}\frac{H_p'}{H_p}\right]e^{ip\phi}$$

$$= \frac{f(\phi)}{R}\left(x_0 i z_1[e^{iz_0}e^{im\phi} - e^{-iz_0}e^{-im\phi}] + x_1[e^{iz_0}e^{im\phi} + e^{-iz_0}e^{-im\phi}] + x_0\sum_{p\neq\pm m} a_p^{(1)}e^{ip\phi}\right)$$

$$+\frac{1}{2}\frac{f^2(\phi)}{R^2}x_0\left(1 + x_0\frac{H_m'}{H_m}\right)[e^{iz_0}e^{im\phi} + e^{-iz_0}e^{-im\phi}], \tag{26a}$$

$$b_m^{(2)}e^{iz_0}e^{im\phi} + b_{-m}^{(2)}e^{-iz_0}e^{-im\phi} + \sum_{p\neq\pm m} b_p^{(2)}e^{ip\phi} = \frac{1}{2}\frac{f^2(\phi)}{R^2}x_0^2(n^2-1)[e^{iz_0}e^{im\phi} + e^{-iz_0}e^{-im\phi}] \tag{26b}$$

from Eqs. (13a) and (13b), respectively. Here, $\partial S_p/\partial x$ and H_p'/H_p are evaluated at x_0. We employ Eq. (26b) first: By introducing the second Fourier harmonics of the boundary function

$$B_q = \frac{1}{2\pi R^2}\int_0^{2\pi} f^2(\phi) e^{iq\phi}\,\mathrm{d}\phi \tag{27}$$

and using the orthogonality of $e^{ip\phi}$ we get

$$b_p^{(2)} = \tfrac{1}{2}x_0^2(n^2-1)[e^{iz_0}B_{m-p} + e^{-iz_0}B_{-m-p}], \tag{28a}$$

$$b_m^{(2)} = \tfrac{1}{2}x_0^2(n^2-1)[B_0 + e^{-2iz_0}B_{-2m}], \tag{28b}$$

$$b_{-m}^{(2)} = \tfrac{1}{2}x_0^2(n^2-1)[B_0 + e^{2iz_0}B_{2m}]. \tag{28c}$$

Next, we calculate x_2, z_1, and $a_p^{(2)}$ from Eq. (26a). Therefore, we first use the orthogonality of $e^{\pm im\phi}$ to get the system of equations

$$\left[-x_2+\frac{x_1^2}{2x_0}\left(1+2x_0\frac{H_m'}{H_m}\right)-\frac{b_m^2}{n^2-1}\frac{H_m'}{H_m}\right]e^{iz_0} = ix_1z_1e^{iz_0}+ix_0z_1[e^{iz_0}A_0-e^{-iz_0}A_{-2m}] + x_1[e^{iz_0}A_0+e^{-iz_0}A_{-2m}]+x_0\sum_{p\neq\pm m}a_p^{(1)}A_{p-m} + \frac{1}{2}x_0\left(1+x_0\frac{H_m'}{H_m}\right)[e^{iz_0}B_0+e^{-iz_0}B_{-2m}], \tag{29a}$$

$$\left[-x_2+\frac{x_1^2}{2x_0}\left(1+2x_0\frac{H_m'}{H_m}\right)-\frac{b_{-m}^2}{n^2-1}\frac{H_m'}{H_m}\right]e^{-iz_0} = -ix_1z_1e^{-iz_0}+ix_0z_1[e^{iz_0}A_{2m}-e^{-iz_0}A_0] + x_1[e^{iz_0}A_{2m}+e^{-iz_0}A_0]+x_0\sum_{p\neq\pm m}a_p^{(1)}A_{p+m} + \frac{1}{2}x_0\left(1+x_0\frac{H_m'}{H_m}\right)[e^{iz_0}B_{2m}+e^{-iz_0}B_0], \tag{29b}$$

which is solved by

$$z_1=-\frac{ie^{2iz_0}}{4A_{-2m}}\left\{\sum_{p\neq\pm m}a_p^{(1)}[e^{-iz_0}A_{p-m}-e^{iz_0}A_{p+m}]-\frac{1}{2}\left(1+2x_0\frac{H_m'}{H_m}\right)[e^{2iz_0}B_{2m}-e^{-2iz_0}B_{-2m}]\right\}, \tag{30}$$

$$x_2=x_0\left\{\frac{1}{2}\left(3[A_0+e^{-2iz_0}A_{-2m}]^2-[B_0+e^{-2iz_0}B_{-2m}]\right)+x_0\frac{H_m'}{H_m}\left([A_0+e^{-2iz_0}A_{-2m}]^2-[B_0+e^{-2iz_0}B_{-2m}]\right) - e^{-iz_0}\sum_{p\neq\pm m}a_p^{(1)}A_{p-m}+2iz_1e^{-2iz_0}A_{-2m}\right\}. \tag{31}$$

Second, we use the orthogonality of $e^{ip\phi}$ in Eq. (26a) to calculate $a_p^{(2)}$ as

$$a_p^{(2)}=\frac{(n^2-1)x_0}{S_p}\left\{[A_0+e^{-2iz_0}A_{-2m}][e^{iz_0}A_{m-p}+e^{-iz_0}A_{-m-p}]\left(\frac{x_0}{S_p}\frac{\partial S_p}{\partial x}-1\right) + \frac{1}{2}\left(1+x_0\left[\frac{H_m'}{H_m}+\frac{H_p'}{H_p}\right]\right)[e^{iz_0}B_{m-p}+e^{-iz_0}B_{-m-p}]+\sum_{k\neq\pm m}a_k^{(1)}A_{k-p}+iz_1[e^{iz_0}A_{m-p}-e^{-iz_0}A_{-m-p}]\right\}. \tag{32}$$

Hence, we have calculated all coefficients in the expansion scheme (14) and therefore are able to calculate the optical modes within the perturbation theory with Eqs. (12a) and (12b). In the following we list remarks about our final second-order results: (i) Since z_1 is complex, see Eq. (30), it strongly affects the chirality in Eq. (15). (ii) For practical evaluations of the formulas it is useful to replace the infinite sums with finite sums, e.g., ranging from $p=-150$ to $p=150$. (iii) In the formulas it is still assumed $A_{-2m}=A_{2m}^{\star}\neq 0$ to allow for a proper evaluation. (iv) Although the boundary conditions are evaluated in second order, the parameter z is just fixed up to the order proportional to λ.

V. APPLICATIONS

In this section we apply the derived formulas to two classes of example systems and demonstrate their validity. In Sec. V A we investigate the spiral cavity and in Sec. V B notched circular cavities are examined.

A. The spiral cavity

In this section we investigate the spiral cavity defined by

$$\frac{r(\phi)}{R}=1-\frac{\epsilon}{2\pi}\phi. \tag{33}$$

This cavity has been studied experimentally and theoretically and exhibits copropagating optical mode pairs with finite chirality even for small notch sizes ϵ [3,30]. Therefore, it is an ideal system to demonstrate the derived formulas.

For the optical modes with $l=1,2,3$ in a spiral cavity with $(\epsilon,n)=(0.04,2.0)$ the predicted values of x are compared to the ones numerically determined in Fig. 2. In general a very good agreement is obtained. Around $\mathrm{Re}\,x=14$ a strong interaction between modes with $l=1$ and $l=2$ is observed. Here, the predictions become slightly less accurate. The origin of this interaction is a quasidegeneracy in $\mathrm{Re}\,x$ and therefore an emerging period-four structure (so-called quasiscar [41]) for

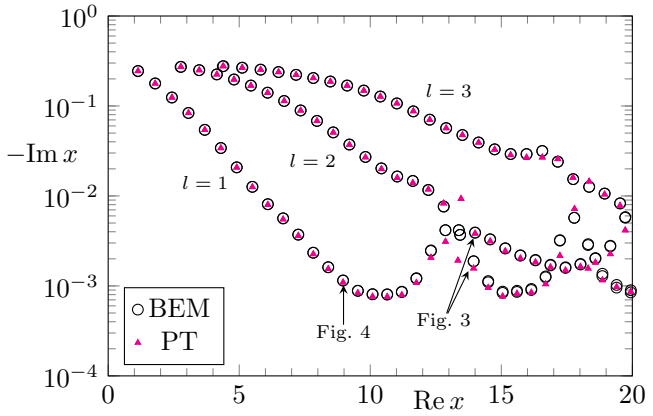

FIG. 2. Second-order perturbation theory results for $x = kR$ values of optical modes with $l = 1,2,3$ in the spiral cavity are shown as magenta triangles. Corresponding BEM results are shown as black open circles. The parameters of the spiral are $(\epsilon,n) = (0.04,2.0)$.

$l = 1$ and $l = 2$ modes, compare to the BEM near-field pattern in Fig. 3(b). This occurrence of the period-four structure is also predicted with perturbation theory; see Fig. 3(a). However, its detailed mode pattern shows slight deviations from the BEM results close to the quasidegeneracy [compare in Fig. 3] and fails where the modes are quasidegenerate (not shown).

On the other hand, in the usual case of separated modes with different mode numbers l not only the $x = kR$ values are predicted well but also the near-field intensity pattern; see Fig. 4 for an example with the mode pair $(m,l) = (14,1)$ with $\mu =$

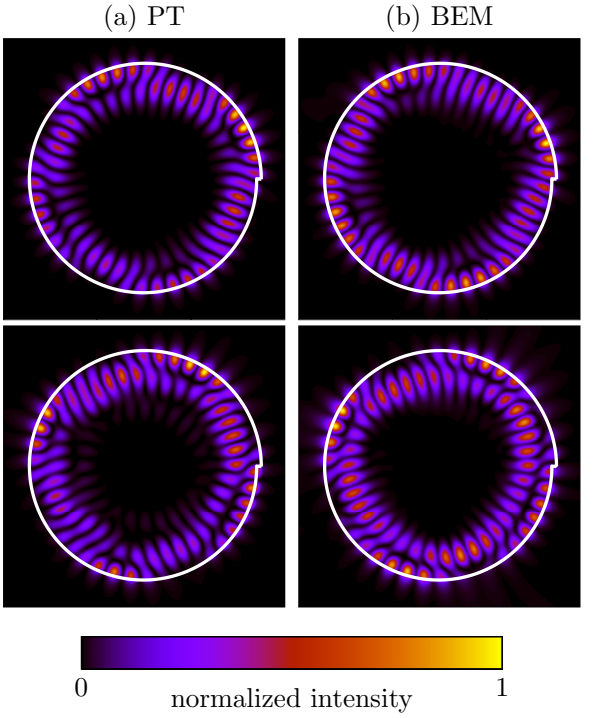

FIG. 3. Near-field intensity pattern of the optical modes with (upper panels) $(m,l) = (23,1)$ and (lower panels) $(m,l) = (19,2)$ in the spiral cavity with $(\epsilon,n) = (0.04,2.0)$. The modes are calculated (a) with perturbation theory and (b) with BEM. The colormap ranges from no intensity (black) to high intensity (bright yellow).

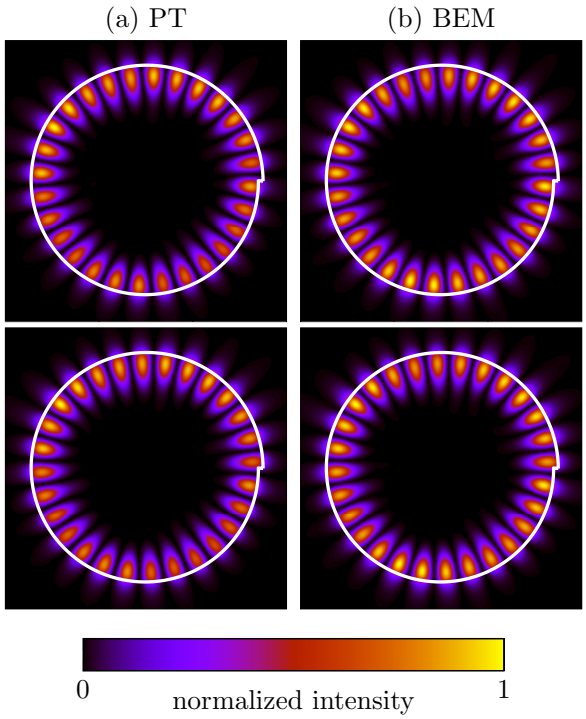

FIG. 4. The near-field intensity pattern of the mode pair with (top panels) $(m,l,\mu) = (14,1,0)$ and (bottom panels) $(m,l,\mu) = (14,1,1)$ in a spiral cavity with $(\epsilon,n) = (0.04,2.0)$ is shown in (a). The corresponding BEM intensity pattern is shown in (b). The colormap ranges from no intensity (black) to high intensity (bright yellow).

0,1. Here, the modes almost look like modes in a circular cavity but note that also the phase of the mode in azimuthal direction is a nontrivial information which is predicted almost precisely.

For the same mode pair as in Fig. 4 the far-field intensity pattern is shown in Fig. 5. Also here a very good agreement of the predicted, Eq. (16), and the numerically determined pattern is observed. Note that all far-field intensity patterns are normalized to the area below the curves.

In the following we keep the mode numbers $(m,l) = (14,1)$ fixed and vary the notch size ϵ of the spiral and thereby the strength of the perturbation. In Figs. 6(a) and 6(b) the real and imaginary part of x for the mode pair is shown. Already first-order results are able to predict $\mathrm{Re}\, x$ well since it is almost proportional to ϵ^1. For a reasonable prediction of $\mathrm{Im}\, x$, second-order perturbation theory is needed to capture the proportionality with ϵ^2. Figure 6(c) shows the chirality of the optical mode pair as function of notch size ϵ. As one expects from ray dynamics [30,41,42,46] the optical modes propagate in the CCW direction. Both modes have the same preferred sense of rotation, i.e., they copropagate. The chirality of both modes increases with increasing notch size. This is surprisingly well described by using only properties proportional to λ, and it is slightly improved by including also $a_p^{(2)}$ to the prediction.

In the following we analyze the error of the perturbation theory with increasing notch size ϵ, i.e., increasing perturbation strength. Therefore we calculate the difference $\delta x = x_{\mathrm{BEM}} - x_{\mathrm{PT}}$ of numerically determined and predicted $x = kR$ values. The results are shown in Fig. 7 for the mode pair with $(m,l) = (14,1)$. As expected the error increases for

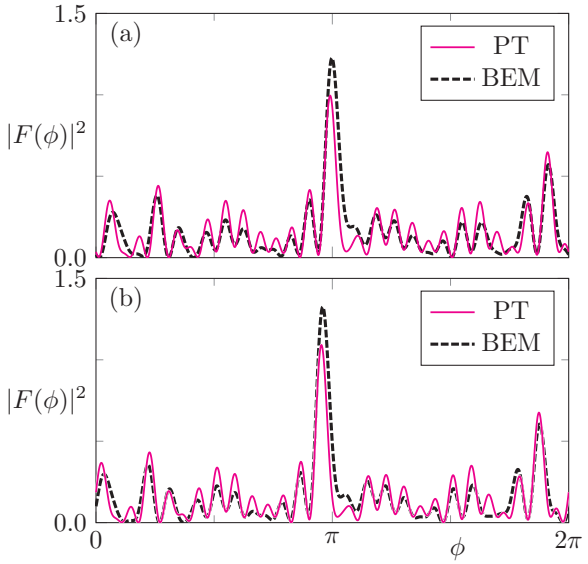

FIG. 5. The far-field intensity pattern $|F(\phi)|^2$, see Eq. (16), of optical modes with (a) $(m,l,\mu) = (14,1,0)$ and (b) $(m,l,\mu) = (14,1,1)$ in a spiral cavity with $(\epsilon,n) = (0.04,2.0)$ is shown as a solid magenta curve. The corresponding BEM result is shown as a dashed black curve. Both intensity patterns are normalized according to the area below the curves.

larger ϵ and is roughly proportional to ϵ^3 which indicates the next (third)-order in a perturbative expansion of x. Note that $\mathrm{Re}\,\delta x$ and $\mathrm{Im}\,\delta x$ contribute equally to the absolute error, but since $\mathrm{Im}\,x \ll \mathrm{Re}\,x$ the relative error of $\mathrm{Im}\,x$ is larger. This is already visible in Figs. 6(a) and 6(b).

Furthermore, we analyze the complex frequency splitting Δx which is also of experimental relevance [47–49] and advantageous for polarization control [50]. The real part of Δx corresponds to the difference in the peak positions of the spectra, and the imaginary part reflects the difference in the line widths of the two modes. As shown in Fig. 8 for the mode pair with $(m,l) = (14,1)$, Δx is dominated by its real part which is almost proportional to ϵ^1. This is predicted correctly by the perturbation theory. The splitting in the imaginary part is very small up to $\epsilon \sim 0.05$ and increases nonlinearly afterwards which is beyond a perturbative description in the second order. Note that in this regime the splitting of the imaginary part is below the error of the perturbation theory; compare to Fig. 7(c).

In the Appendix we present an improvement of the perturbation theory using a scaling of the boundary. This procedure is demonstrated at the spiral cavity.

B. The notched circular cavity

The second class of systems we study here is the notched circle defined by the boundary

$$\frac{r(\phi)}{R} = 1 + \sum_{\nu=0}^{N_\nu} \sum_{\xi=-\infty}^{\infty} \epsilon_\nu \exp\left(-\frac{(\phi - \phi_\nu - 2\pi\xi)^2}{2\sigma_\nu^2}\right), \quad (34)$$

where N_ν is the number of notches each is placed at an angle ϕ_ν and each has a width parameter $\sigma_\nu > 0$. Note, since $\sigma_\nu \ll 1$, it is numerically sufficient to use just a few terms in the sum over ξ, e.g., $\xi \in \{-1,0,1\}$.

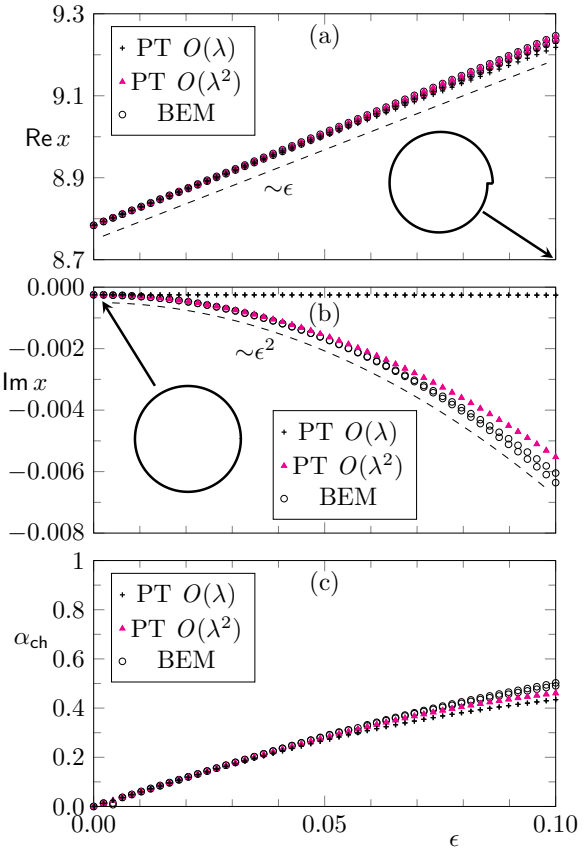

FIG. 6. The (a) real and (b) imaginary part of $x = kR$ is shown as a function of notch size ϵ for the optical modes with $(m,l,\mu) = (14,1,0)$ and $(m,l,\mu) = (14,1,1)$. (c) shows the chirality, Eq. (15), of the modes vs notch size ϵ. Black crosses and magenta triangles correspond to first- and second-order perturbation theory, respectively. BEM results are shown as black open circles. The refractive index of the spiral cavity is $n = 2.0$. Insets show the boundary of the cavity for $\epsilon = 0.0$ and $\epsilon = 0.1$. A dashed curve illustrates the scaling with (a) ϵ and (b) ϵ^2.

Single-notched cavities have been reported to show unidirectional light emission, see, e.g., [2] for a notched ellipse. In the case of a symmetric local boundary perturbation as, e.g., in a single-notched circular cavity, the perturbation theory from Dubertrand *et al.* [19] can be simplified [21].

Two (and more) notches have been used to select the lasing mode in a cavity, i.e., to spoil the Q factor of undesired modes [44]. Furthermore, a fine tuning of the position and size of the local perturbations allow for an investigation of EPs [35,43]. Near an EP the mode pair exhibits a strong chirality, see Eq. (15), and becomes sensitive to slight boundary perturbations. Although this sensitivity is valuable, e.g., for sensors, it results in larger deviations between perturbatively predicted and numerically determined modes close to an EP.

In this paragraph we first investigate a cavity far away from an EP. Therefore we fix the parameters of two notches in Eq. (34) to $(\epsilon_1,\sigma_1) = (-0.08,0.07)$, and $(\epsilon_2,\sigma_2) = (-0.09,0.03)$; see Fig. 1(d). The angle $\phi_1 = 0$ of the first notch is fixed and the angle ϕ_2 of the second notch is varied. The results for x of the optical modes $(m,l) = (8,1)$ are shown in

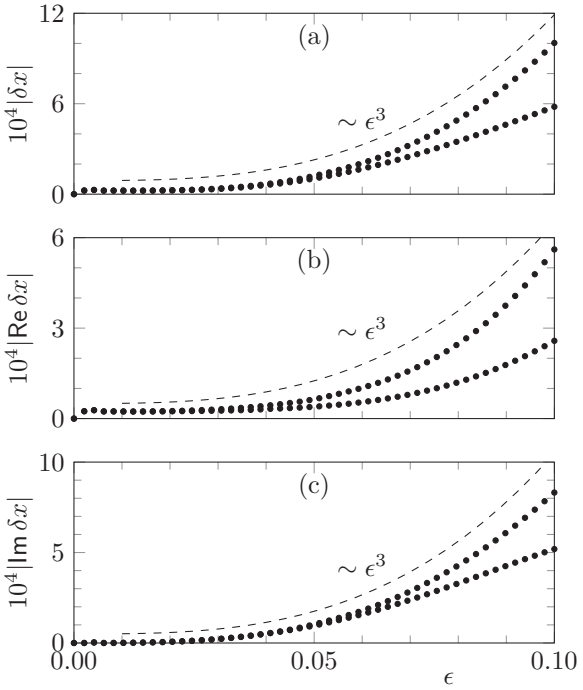

FIG. 7. The error of second-order perturbation theory for the mode pair $(m,l) = (14,1)$ in a spiral cavity with refractive index $n = 2.0$ is shown as function of notch size ϵ (black dots).

Figs. 9(a) and 9(b). Here, the predicted values of x are in a very good agreement with numerical (BEM) results. Around $\phi_2 \sim 1.35$ where the two modes come close in x, the chirality α_{ch} is enhanced; see Fig. 9(c), which is well described by the perturbation theory.

Next, we tune the system closer to an EP for the mode pair $(m,l) = (10,1)$ by changing the parameters of the notches to $(\epsilon_1,\sigma_1) = (-0.056,0.06)$ and $(\epsilon_2,\sigma_2) = (-0.06,0.035)$. The angle $\phi_1 = 0$ is fixed and the angle ϕ_2 is again varied. The results for x and the chirality α_{ch} of the mode pair

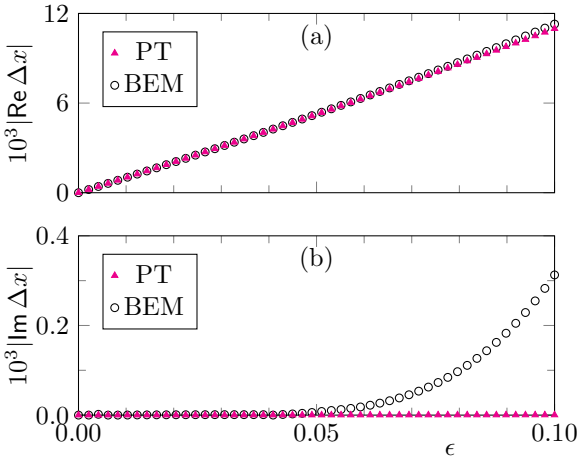

FIG. 8. Black open circles (BEM) and magenta triangles (second-order perturbation theory) show the (a) real and (b) imaginary part of the splitting of the optical mode pair $(m,l) = (14,1)$ in a spiral cavity with $n = 2.0$.

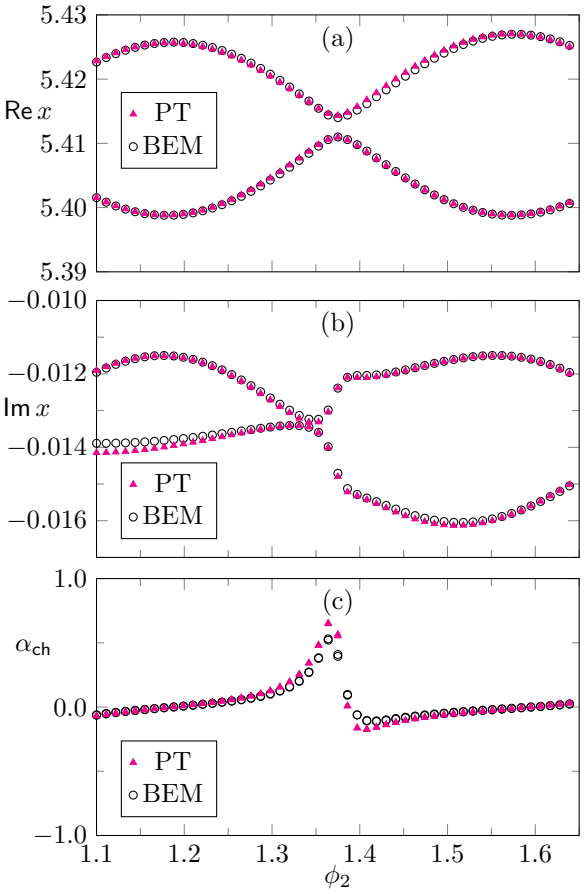

FIG. 9. The (a) real and (b) imaginary part of $x = kR$ is shown as function of the angle ϕ_2 for the mode pair with $(m,l) = (8,1)$ in the double-notched cavity with $n = 2.0$. (c) shows the chirality, Eq. (15), of the modes vs angle ϕ_2. Magenta triangles represent second-order perturbation theory and BEM results are shown as black open circles.

$(m,l) = (10,1)$ are compared to BEM results in Figs. 10(a) to 10(c). Again an overall good agreement is observed over a large range of ϕ_2. But close to two EPs near $\phi_2 = 1.1$ some structural differences occur: (i) In $\mathrm{Re}\,x$ the perturbation theory predicts a crossing while BEM does not; see inset in Fig. 10(a). Therefore, the system is not exact on the EP but very close to it. (ii) The crossing in $\mathrm{Im}\,x$ is predicted for different angles and its curve shape between the predicted EPs is different; see inset in Fig. 10(b). (iii) Perturbation theory predicts a sudden drop in the chirality while BEM calculations suggest a smooth transition from $\alpha_{\mathrm{ch}} \approx 1$ to $\alpha_{\mathrm{ch}} \approx -1$; see insets in Fig. 10(c). Therefore, we suggest that EPs limit the perturbation theory presented here. Note that it is intuitive that the perturbation theory breaks down close to an EP because there two modes coalesce which is the strongest deviation from the unperturbed symmetric case where both modes are orthogonal. Nevertheless, for system parameters away from the EP the mode properties are predicted well.

To compare our perturbation theory for asymmetric cavities with the formulas derived by Dubertrand *et al.* [19] for symmetric cavities, we investigate a double-notched circle where both notches have the same width parameter $\sigma_1 = \sigma_2 = 0.035$ and fixed $\epsilon_1 = -0.06$ and $(\phi_1,\phi_2) = (0,1.375)$.

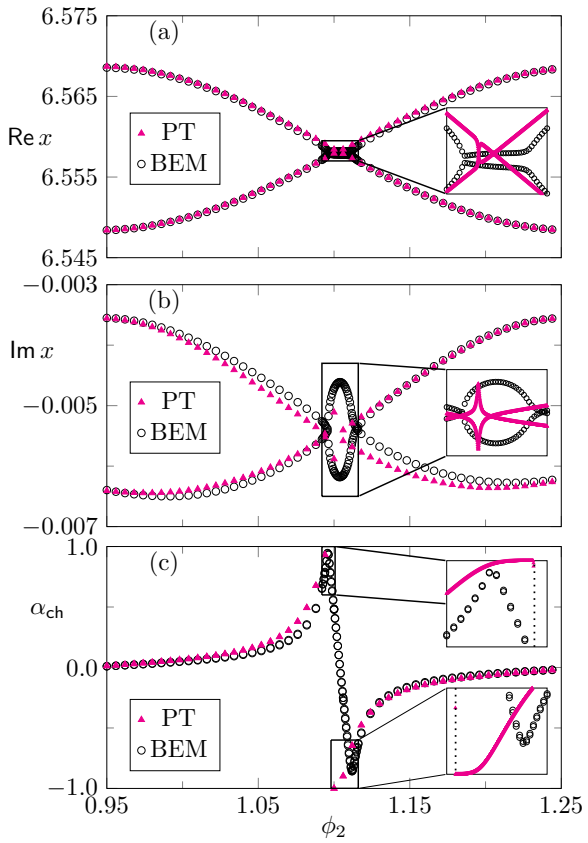

FIG. 10. The (a) real and (b) imaginary part of $x = kR$ is shown as function of the angle ϕ_2 for the mode pair with $(m,l) = (10,1)$ in the double-notched cavity with $n = 2.0$. (c) shows the chirality, Eq. (15), of the modes vs angle ϕ_2. Second-order perturbation theory results are shown as magenta triangles and BEM results are shown as black open circles. A dotted black line in the insets of (c) at $\phi_2 = 1.0996$ is a guide to the eye.

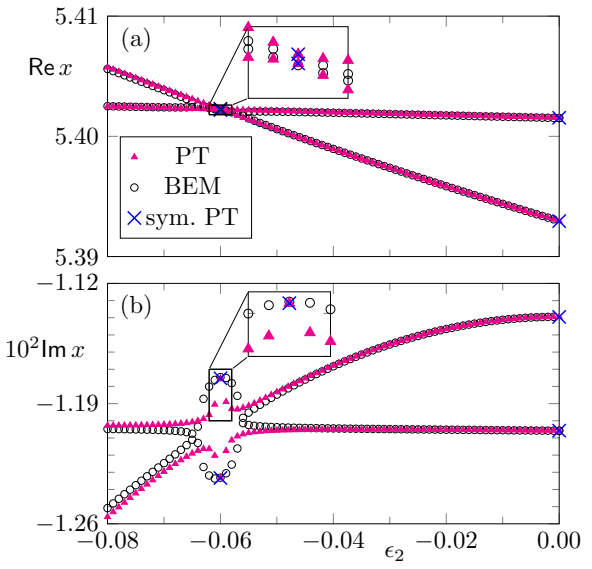

FIG. 11. The (a) real and (b) imaginary part of $x = kR$ for the mode pair $(m,l) = (10,1)$ is shown as a function of the size ϵ_2 of the second notch. Both notches have the same width parameter $\sigma_1 = \sigma_2 = 0.035$. For $\epsilon_2 = -0.06$ (two notches of equal size) and $\epsilon_2 = 0$ (a single notch), perturbation theory for symmetric deformations [19] can be applied (blue crosses). Second-order perturbation theory results for asymmetric cavities, Eqs. (23) and (31), are shown as magenta triangles and BEM results are shown as black open circles.

Varying ϵ_2 allows us to cover the case of a symmetric cavity for $\epsilon_2 = -0.06$ and $\epsilon_2 = 0$. As shown in Figs. 11(a) and 11(b), employing Eqs. (23) and (31) for symmetric cavities results in the same values for x as predicted by Dubertrand *et al.*; see blue crosses. Additionally, our perturbation theory shows a good agreement to numerically determined values also for other ϵ_2 where the cavity is asymmetric.

VI. CONCLUSION AND OUTLOOK

In this paper we derived analytical formulas for optical modes in slightly deformed microdisk cavities. Our calculations are based on a perturbative expansion of the boundary conditions up to second order in the perturbation parameter. In contrast to the previous work by Dubertrand *et al.* we extended the theory to a degenerate perturbation theory applicable to cavities without a mirror-reflection symmetry. We show the validity of the derived formulas at two example systems: a spiral cavity and a notched circular cavity. In both cases we observe a good agreement to numerically exact solutions with the BEM. Furthermore, we demonstrated that scaling the cavity size can be used to minimize the area of perturbation which results in an improved prediction of complex wave numbers.

In the following we list some advantages and disadvantages of the derived formulas: (i) A disadvantage of the formulas is that they fail for special combinations of mode numbers and boundary shapes, i.e., if the Fourier harmonic A_{2m} of the boundary deformation function vanishes the formulas cannot be evaluated properly. (ii) Close to exceptional points the predictions become inaccurate, e.g., the chirality changes discontinuously. Note that this is a natural feature of an exceptional point where small changes in a parameter have a large effect on the involved modes. (iii) Our perturbation theory works also for cavities with chaotic ray dynamics as long as the deformation area is small. (iv) Especially in the spiral cavity the boundary function $r(\phi)$ is not continuous at the notch but in the perturbation theory the Fourier harmonics of the deformation function enter which always represent a contiguous version of the boundary. Our results suggest that this can be seen as a mathematical detail without effecting the obtained results strongly. (v) The derived formulas are an analytical proof that mode pairs are copropagating with a finite chirality if the cavity's boundary is deformed asymmetrically. (vi) The numerical effort of evaluation is very low in comparison to the BEM which allows, e.g., parameter studies or to use them as an initial guess for precise numerical methods. (vii) The presented scaling improvement is easy to implement and can result in valuable enhanced accuracy.

The derived formulas provide a foundation to generalize the inverse problem [39] to find optimal boundary shapes for generic far-field intensity patterns. This will be part of future work. Another future challenge is the derivation of appropriate formulas for TE modes. The simplification of the presented formulas for local boundary perturbations as done in Ref. [21] for the symmetric case is also under consideration.

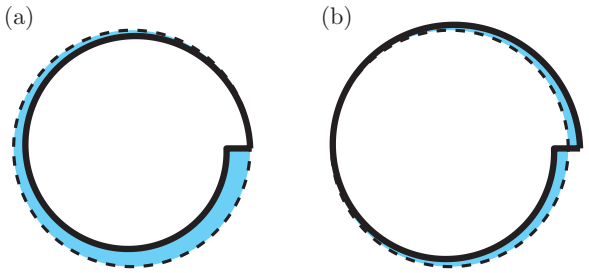

FIG. 12. (a) Spiral cavity with $\epsilon = 0.2$ and (b) rescaled spiral cavity with η as in Eq. (A4) is shown as a black solid curve. The dashed curve is a circle of radius R, and the cyan filled region illustrates the area δa where the deformation function changes the refractive index.

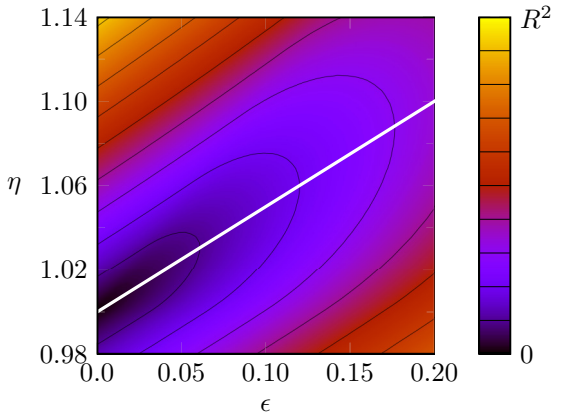

FIG. 13. Area of the perturbation δa depending on notch size ϵ of the spiral and the scaling factor η is color encoded from dark (small perturbation area) to bright (large perturbation area). Black solid curves are contour lines. The white line is the optimal scaling to minimize the perturbation area; see Eq. (A4).

ACKNOWLEDGMENTS

We thank M. Kraft and C.-H. Yi for discussions. Financial support from DFG (Project No. WI 1986/6-1) is acknowledged.

APPENDIX: IMPROVING PERTURBATION THEORY USING SCALING

In this Appendix we explain how a rescaling of the cavity size can be used to get an improved perturbative prediction of $x = kR$. This improvement is valuable in cases where the boundary perturbation function $f(\phi)$ enlarges (or reduces) the overall cavity size. A typical example is the spiral where $f(\phi) < 0$ for all $\phi > 0$.

The key idea of the scaling improvement is not to use $r(\phi)$ directly but to introduce a rescaled radius $r_\eta(\phi)$

$$r_\eta(\phi) = \eta r(\phi) \tag{A1}$$

of the cavity. Consequently, the rescaled boundary deformation function is

$$f_\eta(\phi) = r_\eta(\phi) - R. \tag{A2}$$

The scaling factor η is then chosen such that it minimizes the area where $f_\eta(\phi)$ changes the refractive index of the circular cavity of radius R; see Fig. 12 for a rescaled spiral with $\epsilon = 0.2$.

Using the rescaled deformation function for the Fourier harmonics A_q and B_q in Eqs. (20) and (27) results in a prediction x_η of the rescaled cavity. Thereby, the complex wave number x of the original nonrescaled cavity is obtained by

$$x = \eta x_\eta. \tag{A3}$$

In the following we illustrate the rescaling improvement at the spiral cavity; see Eq. (33). First, we have to deduce the optimal scaling η for a given notch size ϵ. Therefore, Fig. 13 shows the perturbation area as function of the scaling factor η and notch size ϵ. The optimal scaling factor is well described by

$$\eta = 1 + \frac{\epsilon}{2}, \tag{A4}$$

which is shown as white line in Fig. 13. Using this scaling factor for the perturbation theory results in a better agreement of the predicted x and determined BEM values as shown in Fig. 14 for the modes $(m,l) = (18,1)$ in the spiral with $n = 2.0$.

Note that additionally to the scaling improvement, also shifting the cavity in the x-y plane can be used to minimize the area of perturbation. This procedure has already been demonstrated in Ref. [20] to be valuable, e.g., for the Limaçon.

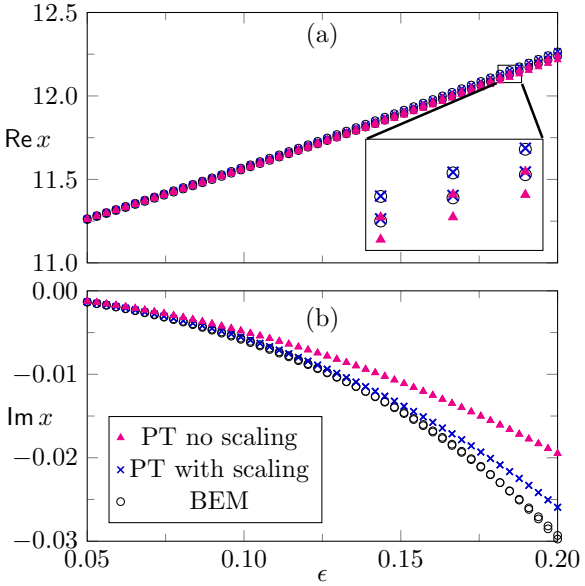

FIG. 14. (a) Real and (b) imaginary part of complex wave number x of the optical modes $(m,l) = (18,1)$ in a spiral cavity with $n = 2.0$ is shown as function of notch size ϵ. Dark blue crosses and magenta triangles represent perturbation theory with [η as in Eq. (A4)] and without ($\eta = 1$) scaling. BEM results are shown as black open circles.

[1] J. Wiersig and M. Hentschel, Phys. Rev. Lett. **100**, 033901 (2008).
[2] Q. J. Wang, C. Yan, N. Yu, J. Unterhinninghofen, J. Wiersig, C. Pflügl, L. Diehl, T. Edamura, M. Yamanishi, H. Kan, and F. Capasso, Proc. Natl. Acad. Sci. U.S.A. **107**, 22407 (2010).
[3] G. D. Chern, H. E. Tureci, A. D. Stone, R. K. Chang, M. Kneissl, and N. M. Johnson, Appl. Phys. Lett. **83**, 1710 (2003).
[4] J. Zhu, S. K. Özdemir, Y.-F. Xiao, L. Li, L. He, D.-R. Chen, and L. Yang, Nat. Photonics **4**, 46 (2010).
[5] F. Vollmer and L. Yang, Nanophotonics **1**, 267 (2012).
[6] L. He, S. K. Özdemir, J. Zhu, W. Kim, and L. Yang, Nat. Nanotechnol. **6**, 428 (2011).
[7] S. Sunada and T. Harayama, Opt. Express **15**, 16245 (2007).
[8] W. W. Chow, J. Gea-Banacloche, L. M. Pedrotti, V. E. Sanders, W. Schleich, and M. O. Scully, Rev. Mod. Phys. **57**, 61 (1985).
[9] B. Little, S. Chu, H. Haus, J. Foresi, and J.-P. Laine, J. Lightwave Technol. **15**, 998 (1997).
[10] N. Stefanou and A. Modinos, Phys. Rev. B **57**, 12127 (1998).
[11] A. Yariv, Y. Xu, R. K. Lee, and A. Scherer, Opt. Lett. **24**, 711 (1999).
[12] H. Schomerus and J. Wiersig, Phys. Rev. A **90**, 053819 (2014).
[13] J. Wiersig, J. Opt. A: Pure Appl. Opt. **5**, 53 (2003).
[14] K. J. Vahala, Nature (London) **424**, 839 (2003).
[15] H. Cao and J. Wiersig, Rev. Mod. Phys. **87**, 61 (2015).
[16] J. U. Nöckel and A. D. Stone, Nature (London) **385**, 45 (1997).
[17] B. Peng, Ş. K. Özdemir, S. Rotter, H. Yilmaz, M. Liertzer, F. Monfi, C. M. Bender, F. Nori, and L. Yang, Science **346**, 328 (2014).
[18] M. Brandstetter, M. Liertzer, C. Deutsch, P. Klang, J. Schöberl, H. E. Türeci, G. Strasser, K. Unterrainer, and S. Rotter, Nat. Commun. **5**, 4034 (2014).
[19] R. Dubertrand, E. Bogomolny, N. Djellali, M. Lebental, and C. Schmit, Phys. Rev. A **77**, 013804 (2008).
[20] M. Kraft and J. Wiersig, Phys. Rev. A **89**, 023819 (2014).
[21] J. Wiersig, Phys. Rev. A **85**, 063838 (2012).
[22] L. Ge, Q. Song, B. Redding, and H. Cao, Phys. Rev. A **87**, 023833 (2013).
[23] J.-B. Shim and J. Wiersig, Opt. Express **21**, 24240 (2013).
[24] M. M. White and S. C. Creagh, J. Phys. A: Math. Theor. **45**, 275302 (2012).
[25] S. C. Creagh and M. M. White, Phys. Rev. E **85**, 015201 (2012).
[26] A. Bäcker, R. Ketzmerick, S. Löck, J. Wiersig, and M. Hentschel, Phys. Rev. A **79**, 063804 (2009).
[27] J. Kullig and J. Wiersig, Phys. Rev. E **94**, 022202 (2016).
[28] Q. H. Song, L. Ge, A. D. Stone, H. Cao, J. Wiersig, J.-B. Shim, J. Unterhinninghofen, W. Fang, and G. S. Solomon, Phys. Rev. Lett. **105**, 103902 (2010).
[29] Q. Song, W. Fang, B. Liu, S.-T. Ho, G. S. Solomon, and H. Cao, Phys. Rev. A **80**, 041807 (2009).
[30] J. Wiersig, S. W. Kim, and M. Hentschel, Phys. Rev. A **78**, 053809 (2008).
[31] T. Kato, *Perturbation Theory for Linear Operators* (Springer, New York, 1966).
[32] W. D. Heiss, Phys. Rev. E **61**, 929 (2000).
[33] C. Dembowski, H.-D. Gräf, H. L. Harney, A. Heine, W. D. Heiss, H. Rehfeld, and A. Richter, Phys. Rev. Lett. **86**, 787 (2001).
[34] C. Dembowski, B. Dietz, H.-D. Gräf, H. L. Harney, A. Heine, W. D. Heiss, and A. Richter, Phys. Rev. E **69**, 056216 (2004).
[35] B. Peng, S. K. Özdemir, M. Liertzer, W. Chen, J. Kramer, H. Ylmaz, J. Wiersig, S. Rotter, and L. Yang, Proc. Natl. Acad. Sci. U.S.A. **113**, 6845 (2016).
[36] J. Wiersig, Phys. Rev. Lett. **112**, 203901 (2014).
[37] P. Miao, Z. Zhang, J. Sun, W. Walasik, S. Longhi, N. M. Litchinitser, and L. Feng, Science **353**, 464 (2016).
[38] X.-Y. Wang, H.-Z. Chen, Y. Li, B. Li, and R.-M. Ma, arXiv:1607.08859 [physics.optics].
[39] M. Kraft and J. Wiersig, Phys. Rev. A **94**, 013851 (2016).
[40] M. Kneissl, M. Teepe, N. Miyashita, N. M. Johnson, G. D. Chern, and R. K. Chang, Appl. Phys. Lett. **84**, 2485 (2004).
[41] S.-Y. Lee, S. Rim, J.-W. Ryu, T.-Y. Kwon, M. Choi, and C.-M. Kim, Phys. Rev. Lett. **93**, 164102 (2004).
[42] S.-Y. Lee, S. Rim, J.-W. Ryu, T.-Y. Kwon, M. Choi, and C.-M. Kim, J. Phys. A: Math. Theor. **41**, 275102 (2008).
[43] M. Kim, K. Kwon, J. Shim, Y. Jung, and K. Yu, Opt. Lett. **39**, 2423 (2014).
[44] A. Schlehahn, F. Albert, C. Schneider, S. Höfling, S. Reitzenstein, J. Wiersig, and M. Kamp, Opt. Express **21**, 15951 (2013).
[45] J. Wiersig, A. Eberspächer, J.-B. Shim, J.-W. Ryu, S. Shinohara, M. Hentschel, and H. Schomerus, Phys. Rev. A **84**, 023845 (2011).
[46] J. Kullig and J. Wiersig, New J. Phys. **18**, 015005 (2016).
[47] H. A. M. Leymann, C. Hopfmann, F. Albert, A. Foerster, M. Khanbekyan, C. Schneider, S. Höfling, A. Forchel, M. Kamp, J. Wiersig, and S. Reitzenstein, Phys. Rev. A **87**, 053819 (2013).
[48] H. Kwak, Y. Shin, S. Moon, S.-B. Lee, J. Yang, and K. An, Sci. Rep. **5**, 9010 (2015).
[49] S. K. Kim, S. H. Kim, G. H. Kim, and Y. H. Lee, J. Korean Phys. Soc. **47**, L397 (2005).
[50] A. Daraei, A. Tahraoui, D. Sanvitto, J. A. Timpson, P. Fry, M. Hopkinson, P. S. S. Guimaraes, H. Vinck, D. Whittaker, M. S. Skolnick, and A. M. Fox, Appl. Phys. Lett. **88**, 051113 (2006).